SUPPLEMENTARY INFORMATIONS

Supplementary Note 1: Switching statistics of multiple labelling

In a three-state switching model, the time-dependent probability of m switching cycles of a single fluorescent dye molecule is [2016_Nieuwenhuizen]:

$$P_m^1 = (1-b)^m \frac{r^m}{m!}\exp(-r) + b(1-b)^{m-1}\sum_{n=m}^{\infty}\frac{r^n}{n!}\exp(-r), \quad (1)$$

where parameters r and b depend on the k_{sw} switching and k_{bl} effective bleaching rates as $r=k_{sw}t$ and $b=k_{bl}/k_{sw}$.

In practice, using immunohistochemical procedures, several fluorescence dye molecules label the target molecule and their common switching pattern provides the detected signal. The number of fluorescence dye molecules depends on the stoichiometry of the labelling. Therefore, it is essential to determine the overall probability of m switching cycles of N independent dye molecules (P_m^N). It can be given as the sum of probabilities of all the possible cases when N molecules generate m switching cycles:

$$P_m^N = \sum_{x_1+x_2+\ldots+x_N=m} P_{x_1}^1 \cdot P_{x_2}^1 \cdot \ldots \cdot P_{x_N}^1 \quad (2)$$

where x_1, x_2, and x_N mark the number of switching cycles can be associated to the 1st, 2nd and nth dye molecules, respectively.

As an example, let us assume that only 2 independent dye molecules label the target molecule and provide m switching cycles. In other words, the total number of switching cycles is m but we do not know how many switching cycles belong to each dye molecules. If the first one was detected x_1 time, the second one must be detected $x_2=m-x_1$ times and the overall probability can be given as the sum of all the possible cases ($P_{x_1}^1 \cdot P_{x_2}^1 = P_{x_1,x_2}$):

$$P_m^2 = \sum_{x_1+x_2=m} P_{x_1}^1 \cdot P_{x_2}^1 \quad (3)$$

In general, all the possible cases can be calculated and can be arranged in a matrix form. In this representation the sum of elements of the mth minor diagonal gives the overall probability of m switching cycles generated by two dye molecules. It can be shown that after a critical cluster size the larger that matrix (the larger the possible number of switching cycles), the smaller the sum of

the minor diagonal elements (smaller the probability of the effective switching cycles). The sums of the minor diagonal elements form a vector and give the probability distribution of the switching cycles.

P_0,0	P_0,1	P_0,2	P_0,3	...	P_0,m
P_1,0	P_1,1	P_1,2	...	P_1,m-1	
P_2,0	P_2,1	...	...		
P_3,0	...	...			
...	P_m-1,1				
P_m,0					

Table S1: Probabilities of all the possible switching cases are arranged in a matrix form.

The method can be generalized further and the probability of *m* switching cycles generated by *N* molecules can be calculated.

It is worth to note that the calculation can be simplified by dividing the *N* number of dye molecules into two independent but known populations (e.g. *K* and *N-K*) with number of switching cycles of *i* and *m-i*, respectively.

$$P_m^N = \sum_{i=0}^{m} P_i^K \cdot P_{m-i}^{N-K}. \tag{4}$$

Supplementary Note 2: Validation of 2D analysis

In this paper all the results and conclusions are based on the evaluation of 2D dSTORM measurements. However, the repair foci inside the nucleus have a 3D spatial distribution. Therefore, the applicability of the used 2D data analysis requires a validation process. A test sample simulator software (TestSTORM [69, 70]) was used to generate the ground truth model and comparative 2D and 3D evaluations were performed on the reconstructed super-resolved images. Images were evaluated from the same aspect (number of clusters, mean number of cluster elements etc.) as they were studied in the main text.

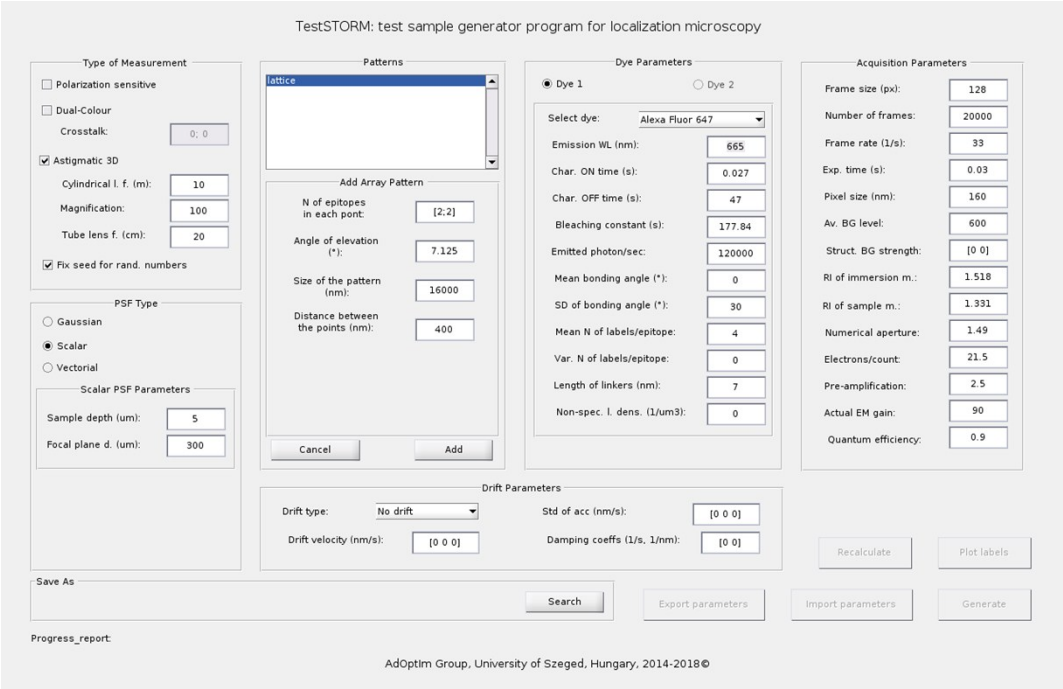

Figure S1. Working GUI window of testSTORM with the used parameters

Simulation parameters were matched to the experimental parameters. The most important parameters are depicted in Figure S1, which shows the working GUI window of the TestSTORM code.

A tilted array pattern (lattice) was defined with the following parameters:

Depth inside the sample: $Depth_{sample}$ =5 µm
Refractive index of the sample: n_{sample} = 1.331
Axial range of the sample: Z_{range}: (-1 µm ,+1 µm)
Axial steps between the adjacent rows: Z_{step} = 50 nm
Distance between the elements (cluster) of the lattice: d = 400 nm
Number of elements in a single column and row: $N_{cluster}/Z_{plane}$ = 41

Number of dye molecules per cluster: 8 dye molecules/cluster
Length of the linker: 7 nm

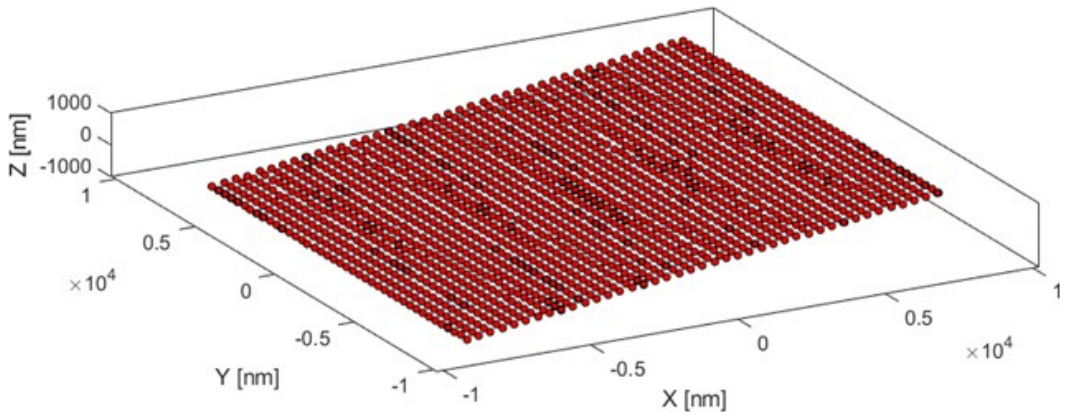

Figure S2. Tilted 3D array pattern consists of 41×41 clusters

A scalar model based on the Pankajakshan-Gibson-Lanni model [2009_Pankajakshan] was applied to calculate the PSF. During the 3D simulations, an additional cylindrical lens with a focal length of 10 m was added to the optical system.

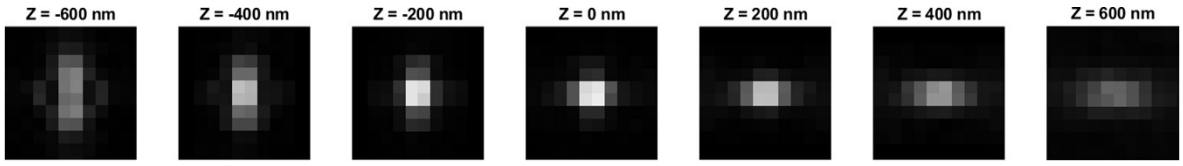

Figure S3. Defocused astigmatic PSF introduced by a cylindrical lens with a focal length of 10 m

High resolution localization images were reconstructed and analysed via the rainSTORM code [71] with the following key parameters:

Thompson precision limit: 25 nm
Applied acceptance radius during the trajectory fitting: $r_{acceptance}$ = 50 nm
Residue threshold: 0.06
Lateral cluster analysis distance parameter: ε_{xy} = 50 nm
Axial cluster analysis distance parameter: ε_z = 100 nm
Minimum number of points in a single cluster: N_{core}=8

Our simulation results prove that 2D and 3D imaging provides identical DOF ranges, i.e. dye molecules in the same axial range (~1 μm) can be associated with the accepted localizations (see Figure S4-a). The slightly reduced number of identified clusters in the 3D case (~7%) is caused by the asymmetry of the PSF. This difference does not affect the trend of the evaluation but

shows that 3D analysis requires a different calibration process. The mean number of cluster elements (see Figure S4-b) shows an approx. 20% reduction in the 3D case in contrast to the 2D one, and the simulations reveal a slight axial dependence in both cases. During the evaluation this axial dependence was neglected, and an average value was applied. Based on these simulation results one can state that 2D measurements (presented in the main text of the paper) provide reliable data and results for the quantitative evaluations. However, determination of 3D specific merit functions (volume of repair foci etc.) and features (structure of repair foci etc.) requires 3D STORM imaging.

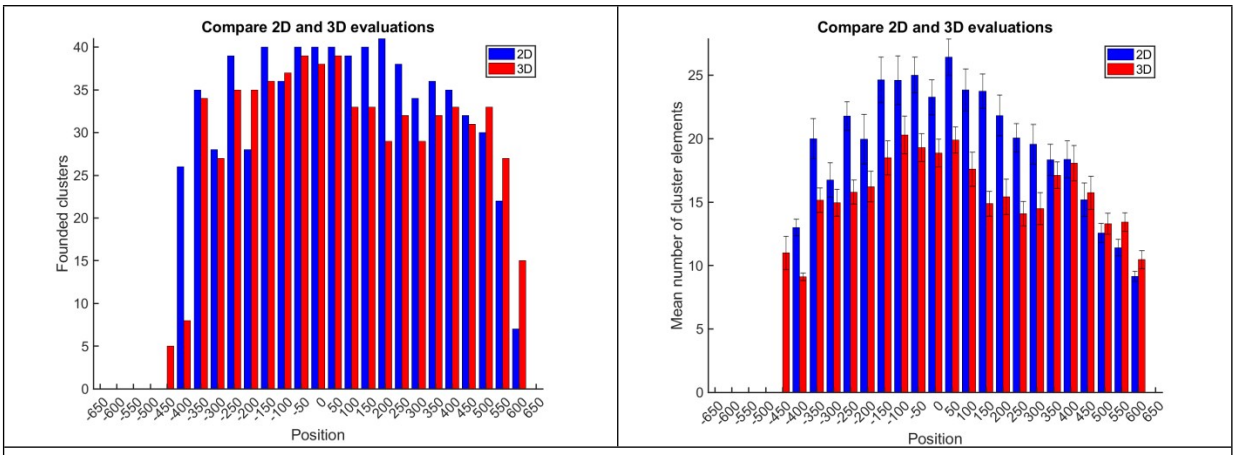

Figure S4. Number of isolated clusters (a) and the mean number of cluster elements as a function of the axial position